JACS
JOURNAL OF THE AMERICAN CHEMICAL SOCIETY
pubs.acs.org/JACS
Article

In-Cell Residue-Resolved NMR of Micromolar α-Synuclein and Tau at 310 K

Hélène Chérot, Théophile Pred'homme, Robert Thai, Frédéric Théodoro, Florence Castelli, and Francois-Xavier Theillet*

Cite This: J. Am. Chem. Soc. 2025, 147, 46259−46269
Read Online

ABSTRACT: Aggregates of nonglobular proteins are associated with several degenerative disorders, e.g., α-synuclein and tau involved in Parkinson's and Alzheimer's diseases. Do these proteins undergo progressive changes in their conformations and interactions in pathologic situations? In-cell NMR provides atomic-scale information in live cells but, until now, only at ∼283 K in the case of unfolded proteins. Here, we report new labeling and acquisition methods enabling in-cell NMR at 310 K to study these proteins at micromolar concentrations, i.e., native cellular abundances. We used stable human cell lines expressing α-synuclein or tau upon induction in a culture medium supplemented with ^{13}C-labeled amino acids, or precursors thereof. Acquiring ^{13}Cα-^{13}CO spectra permitted an early residue-resolved analysis of α-synuclein and tau at 310 K and <10 μM in HEK cells at 700 MHz. We detected disordered conformations and patterns of extended cellular interactions for α-synuclein wild-type and two mutants (F4A, A30P), which suggests the appearance of a subpopulation binding to lipid membrane at 310 K. Only the disordered N-terminus of tau was observable, even upon microtubule dismantling by colchicine. This shows that supplementary binding partners interfere with tau in cells. Our approach offers an excellent scalability, in signal, and resolution, up to 1.2 GHz. ^{13}C-labeling and ^{13}C-detected NMR spectroscopy in live human cells are thus viable techniques for in-cell structural biology.

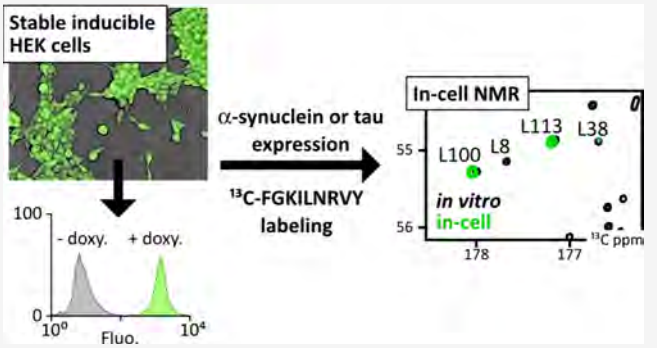

INTRODUCTION

In-cell structural biology provides information about the conformational behaviors and binding abilities of proteins or nucleic acids in cellular milieus. This field is emerging thanks to the development of a range of complementary techniques, including cryo-electron tomography, EPR, mass spectrometry, NMR, or FRET.[1−9] In-cell NMR exploits isotope filters to observe selectively ^{13}C-, ^{15}N-, or ^{19}F-labeled peptides (or nucleic acids) either delivered or transiently expressed in cells, which contain 1% or less of these isotopes at natural abundance.[1,10]

NMR spectroscopy has notably the unique capacity to extract atomic-scale information on local structures and interactions of intrinsically disordered (regions of) proteins (IDRs/IDPs),[11,12] a class of natively nonfolded peptides representing about 30% of eukaryotic proteomes and a great variety of key functions in cells.[13−15] IDPs lack stable 3D structures, which makes them malleable objects,[15,16] whose structural behavior in cells is thus to be questioned.[17,18] This is especially true for those IDPs, whose misfolded forms are important actors of neurodegenerative disorders, like α-synuclein (α-syn) and tau.[19−21]

Atomic-scale studies on IDPs using in-cell NMR have been reported by us and others, showing that unfolded states can be stable in human cells.[1,22−24] However, these analyses were carried out in live cells maintained at 283 K or less: they were based on the observation of backbone amide ^{1}H−^{15}N NMR signals of ^{15}N-labeled IDPs, signals that weaken and overlap severely at physiological pH and temperature, owing to fast water-amide ^{1}H exchange (>25 Hz).[11,25−28] This is unfortunate, because IDPs' conformational ensembles are temperature-dependent,[29−31] and molecular activities of human cells are obviously limited at 283 K.

Other NMR approaches have been developed recently for protein backbone analysis providing residue-specific information on IDPs, which are unaffected by water-amide ^{1}H exchange in physiological conditions.[32−35] Among these, 2D ^{13}Cα-^{13}CO correlation experiments appeared the most suited

Received: August 29, 2025
Revised: November 20, 2025
Accepted: November 21, 2025
Published: December 4, 2025

https://doi.org/10.1021/jacs.5c15061
J. Am. Chem. Soc. 2025, 147, 46259−46269

to in-cell NMR studies: (i) they would not be affected by the broad cellular $^{1}H_2O$ signal, (ii) they would permit a clean isotope filter, and (iii) they would offer decent signal-to-noise ratios for IDPs. The feasibility of using $^{13}C\alpha$-^{13}CO in-cell NMR experiments was still questionable because of the typical line-broadening encountered with in-cell samples, which provokes peak overlaps and information losses.[1]

To get closer to genuine cellular conditions, we set out to establish a consistent approach to generate and analyze in-cell NMR samples, using stable-inducible cell lines, homemade culture media supplemented with isotope-labeled amino acids, and $^{13}C\alpha$-^{13}CO NMR. We present below the step-by-step tests of this in-cell NMR scheme and demonstrate its feasibility and potential usefulness.

RESULTS AND DISCUSSION

Stable HEK Cell Lines with Inducible Expression of α-Synuclein or Tau. We sought to set up an in-cell NMR approach using protein expression in situ, avoiding the nowadays more popular delivery of purified isotope-labeled material.[1] We wanted to avoid transient transfection, too, which provokes broadly inhomogeneous cell populations with regard to protein expression (Figure 1a). We aimed at expressing proteins of interest in an inducible fashion: this would allow temporary isotope-labeling during protein expression, which would minimize the NMR signal from the cellular background. We chose to use a commercial HEK cell line, namely, Flp-In T-Rex 293, which permits to insert a gene of interest (GOI) in a single transcriptionally active locus of the genome under the control of a doxycycline-regulated, hybrid CMV/$TetO_2$ promoter (Figure 1b). This enables a homogeneous strong expression (Figure 1a) upon supplementation with doxycycline at 10 ng/mL (Figure S1a)—which is way below the ∼5 μg/mL of doxycycline necessary to interfere with exogenous α-synuclein aggregation in cells.[36] We selected stable cell pools using hygromycin and obtained nonclonal inducible cell lines for various α-syn and tau constructs. These expressed very reproducible quantities after 48 h of exposure to doxycycline. The intracellular concentrations reached only 9.5 μM for α-syn (Figure 1c) but about 50 μM for tau (Figure S1c). The range of their native concentrations are 40 and 5 μM, respectively[37,38] (or ∼3 and ∼1 copies per 1000 protein molecules in the human brain according to https://pax-db.org/).[39] The molecular content of these cells was also reproducible, hence, generating a constant cellular background NMR signal. This enabled us to obtain background-free spectra, by subtracting spectra recorded with noninduced cells to those recorded with induced cells (Figure 1d).

Amino Acid-Specific Isotope Labeling of Stable-Inducible HEK Cells. HEK cells are standardly cultured in a classical DMEM, the recipe of which is public. Hence, we could emulate it and control the content in amino acids, eventually ^{13}C- and/or ^{15}N-labeled (Table S1). Earlier, in-cell NMR studies have achieved protein isotope-labeling in mammalian cells using uniform ^{15}N-labeling, which is conveniently obtained using commercial culture media (∼100−200 € per sample).[1,10] Amino acid-specific ^{13}C-/^{15}N-labeling could be a cheaper approach, also avoiding peak overlaps in IDPs, which we sought to test on our stable-inducible cell lines. A number of metabolic pathways are off in human cells (https://www.genome.jp/pathway/hsa01230), which might give access to novel labeling schemes for NMR.

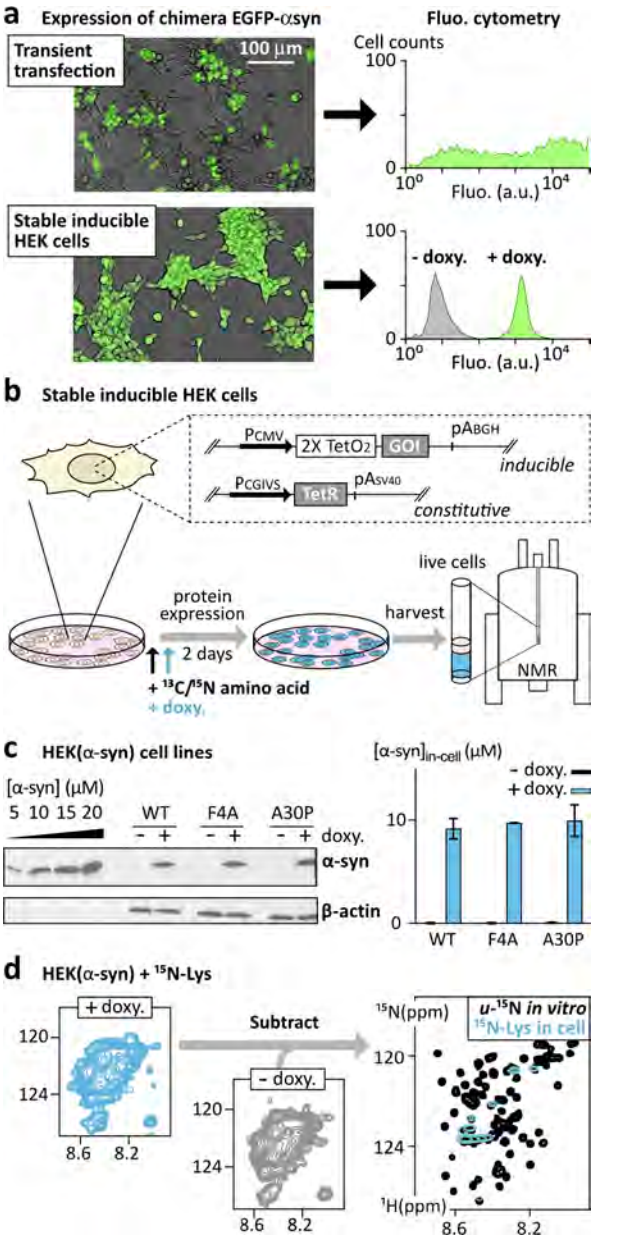

Figure 1. Principles of the sample preparation. (a) Expression of a chimera construct EGFP-α-syn in HEK cells using transient transfection or a stable-inducible HEK cell line (single-locus insert): *left*: overlay of brightfield and fluorescence microscopy; *right*: fluocytometry from transfected HEK cells (*up*) and noninduced (-doxycycline, gray) or induced (+doxy., green) stable-inducible HEK cells (*down*). (b) Our stable-inducible HEK cell lines contain GOIs inserted in a single chromosomal locus repressed by TetR on the *tet* operator 2 $TetO_2$; TetR is released upon binding to doxy., which triggers GOI expression; cells grow in a standard medium, are transferred into a homemade medium containing selected ^{13}C- and/or ^{15}N-labeled amino acids, doxy.-induced 4 h later, and incubated during 48 h before harvesting. (c) Semiquantitative Western-blotting of α-syn showing comparable protein levels in-cell lines expressing α-syn-WT, F4A, or A30P; the histogram shows results from triplicates. (d) Spectra recorded with noninduced cells serve to subtract the cellular background signals from natural abundance ^{13}C/^{15}N-species or from those produced during the incubation in the presence of ^{13}C-/^{15}N-amino acids.

We started with cells expressing α-syn because it yields intense NMR signals. We converged to the following

https://doi.org/10.1021/jacs.5c15061
J. Am. Chem. Soc. 2025, 147, 46259−46269

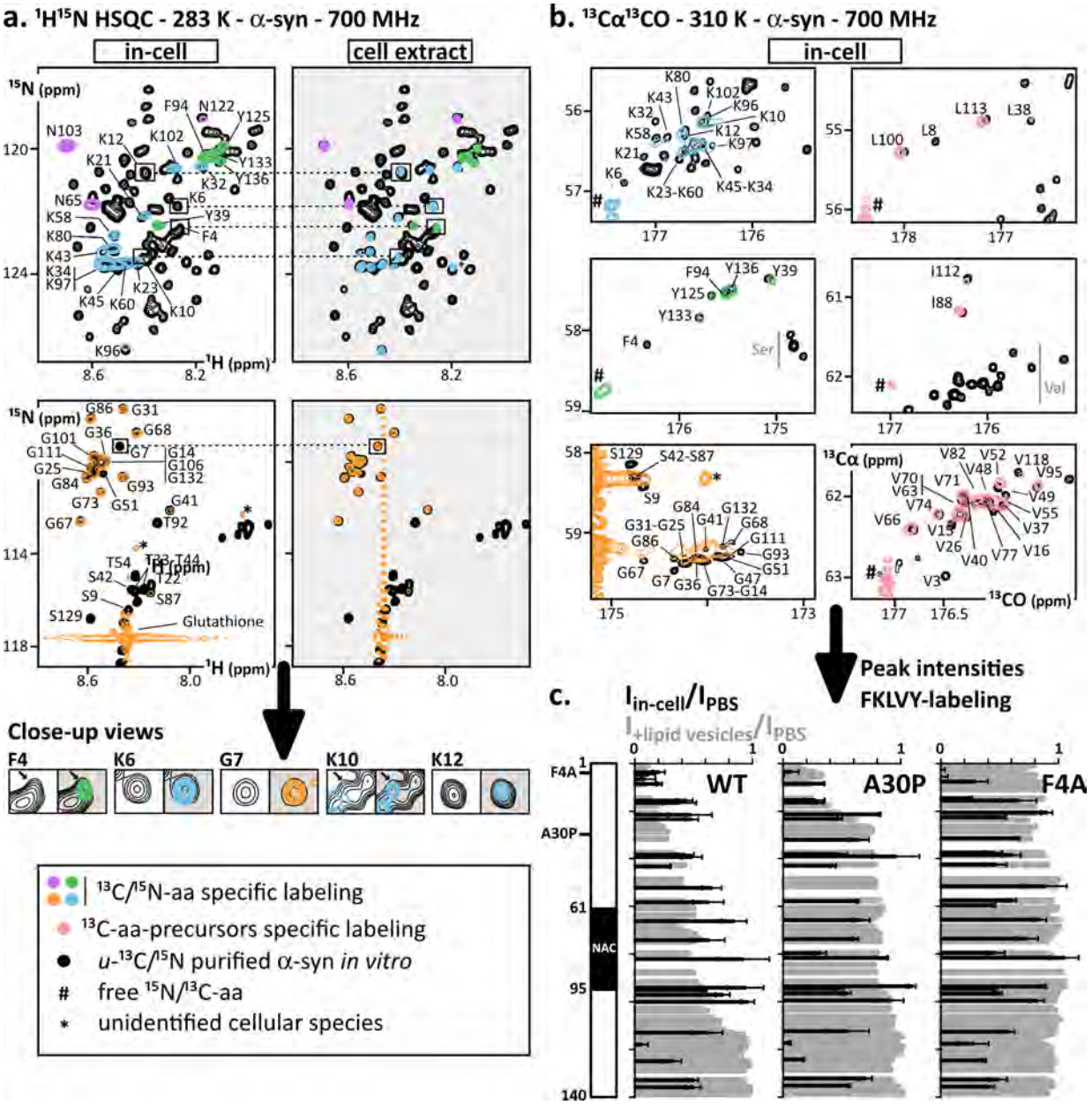

Figure 2. Amino acid-specific isotope labeling and analysis of α-syn in-cell. (a) Overlay of 2D $^{1}H-^{15}N$ HSQC spectra of purified [u-^{15}N]-α-syn (black) and of cells expressing α-syn in the presence of ^{15}N-Asn (purple), ^{15}N-Lys (blue), ^{15}N-Phe/^{15}N-Tyr (green), or ^{15}N-Gly (yellow) (spectra from noninduced cells were subtracted); spectra were recorded on intact cells or in clarified cell extracts (after sonication and a brief boiling step). (b) Overlay of 2D $^{13}C\alpha$-^{13}CO spectra of purified recombinant [u-^{13}C]-α-syn (black) and of cells expressing α-syn in the presence of ^{13}C-Lys (blue), ^{13}C-Phe/^{13}C-Tyr (green), ^{13}C-Gly, or ^{13}C-precursors of Leu, Val, or Ile (pink) (spectra from noninduced cells were subtracted). (c) *Black:* residue-specific peak intensity ratios in $^{13}C\alpha$-^{13}CO spectra of cells expressing $^{13}C-$F/K/L/V/Y-labeled α-syn-WT/A30P/F4A versus purified α-syn in PBS ($I_{in\text{-}cell}/I_{PBS}$) along the primary structure at 310 K; gray: residue-specific peak intensity ratios in $^{13}C\alpha$-^{13}CO spectra of [u-^{13}C] α-syn in the presence of pig brain polar lipid vesicles at 4 g/L (see Figure S5) purified, isolated α-syn in PBS ($I_{+lipid\ vesicles}/I_{PBS}$) at 310 K.

experimental scheme: we switch to a culture medium containing selected ^{13}C-/^{15}N-amino acids 4 h before inducing α-syn expression and then incubate 48 h before harvesting cells. We carried out successfully ^{15}N-labeling of Asn, Lys, Phe, and Tyr residues without any marked scrambling in 2D $^{1}H-^{15}N$ HSQC in-cell NMR spectra at 283 K (Figure 2a). We also succeeded in incorporating ^{15}N-Gly in α-syn, although Gly scrambles partially with Ser amino acids. This pushed us to remove Ser from the culture medium, which resulted in robust ^{15}N-Gly and partial ^{15}N-Ser labeling. After subtraction of a spectrum from noninduced cells, the observed crosspeaks have the chemical shifts of purified α-syn, with intensities modulated by the in-cell environment (see below). At the opposite, supplementing the culture medium with ^{15}N-Asp, -Leu, -Val, or -Ile yielded a widespread of amide ^{15}N signals, i.e., no selective labeling of those amino acids (Figure S2). These results are in agreement with the common $^{2}D/^{13}C/^{15}N$-Lys/Arg labeling in SILAC-MS for quantitative proteomics,[40] and with the handful of NMR-related reports about amino acid-specific ^{15}N- labeling in transiently transfected mammalian cells.[41−44]

Consistently with the results from ^{15}N-labeling assays, we observed efficient incorporations of ^{13}C-Asn, -Lys, -Phe, and

https://doi.org/10.1021/jacs.5c15061
J. Am. Chem. Soc. 2025, 147, 46259−46269

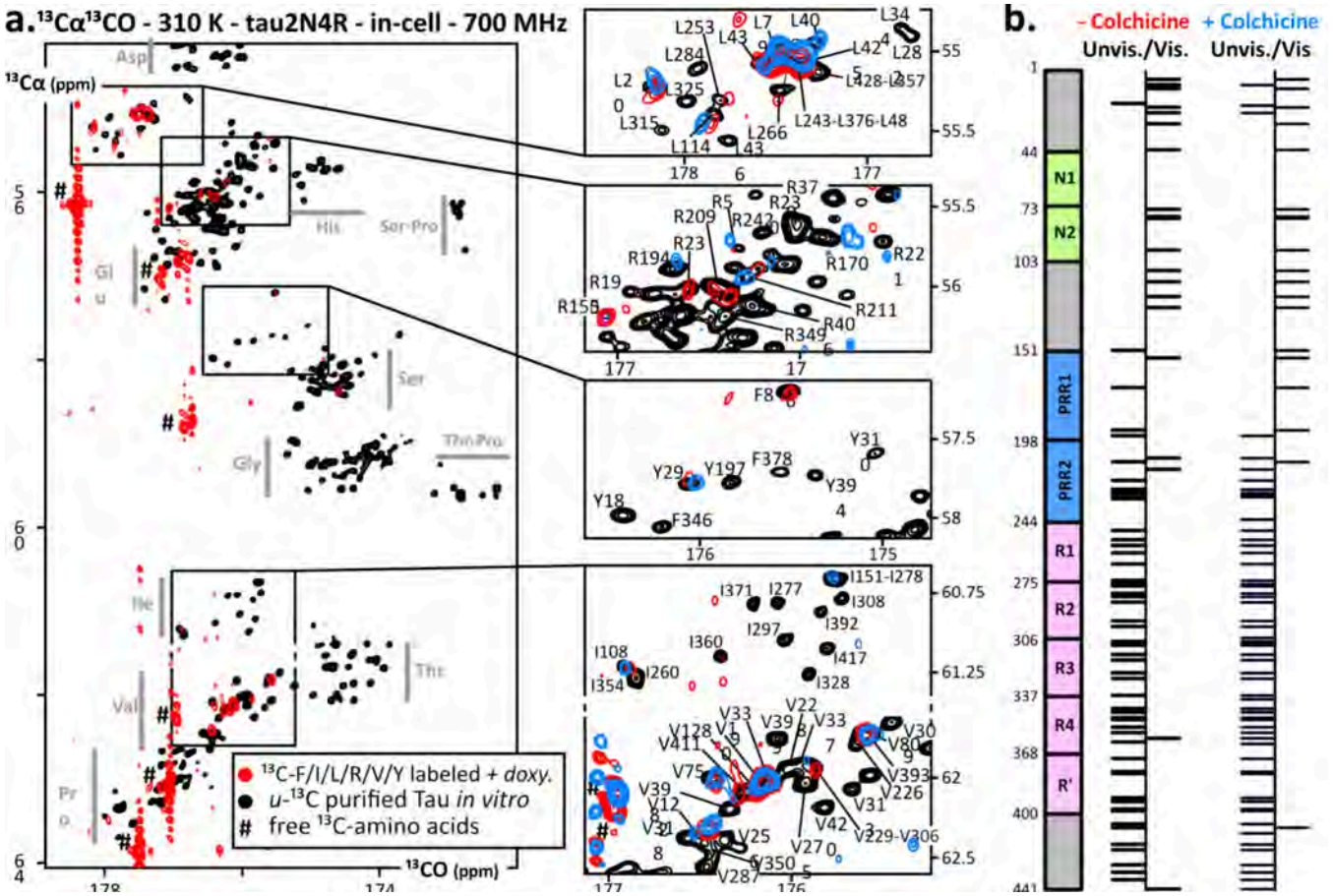

Figure 3. In-cell NMR of tau2N4R expressed in situ. (a) Overlay of 2D ^{13}Cα-^{13}CO spectra of purified recombinant [u-^{13}C]-tau (black) and of cells expressing ^{13}C−F/I/L/R/V/Y tau in absence (red) or in the presence of colchicine (blue) (spectra from noninduced cells were subtracted); cells use ^{13}C-Arg to produce some ^{13}C-Pro. (b) Scheme of tau2N4R primary structure (441 residues) and summary of peaks that are unambiguously detected or nondetected.

-Tyr with no scrambling issues, and of ^{13}C-Gly resulting also in partial ^{13}C-Ser labeling. These permitted the first ^{13}C-detected in-cell protein NMR spectra in human cells at 310 K, using 4 h-long ^{13}Cα-^{13}CO experiments at 700 MHz (Figures 2b and S3). These revealed crosspeaks corresponding to those of purified, isolated α-syn in vitro. Interestingly, we did not have to carry out any background subtraction for ^{13}C-Phe/Tyr, with the cellular signal being below the noise level.

Then, building on the observation that amide nitrogen atoms of Leu/Val/Ile were readily exchanged and diluted in the cellular content, we thought to use their ^{13}C-labeled precursors α-ketoisocaproate, α-ketoisovalorate, and 2-keto-3-methylvalerate, respectively (Figure S2). These cheaper alternatives were effectively converted into their amino acid counterpart and permitted to record in-cell NMR ^{13}Cα-^{13}CO spectra of α-syn at 310 K, which showed exclusively Leu, Val, or Ile signals (Figures 2b and S3). These results are in agreement with very recent labeling studies on transiently transfected suspension HEK cells.[45−47] 2D ^{1}H−^{13}C HSQC spectra revealed that these ^{13}C-amino acids, or precursors thereof, were not or very weakly processed into undesired metabolites (Table S2), except for ^{13}C-Gly incorporated in glutathione as already reported.[48]

We evaluated the isotopic incorporation levels in our conditions, i.e., induced expression in HEK cell lines previously grown at natural abundance, using purified α-syn treated by acid hydrolysis. Mass spectrometry analysis revealed incorporation levels of about 80% for Leu, Phe, and Val and about 90% for Lys and Tyr (Table S4).

Altogether, we succeeded in incorporating a number of ^{13}C- or ^{15}N-amino acids during the expression of a GOI in stable-inducible HEK cells. This incorporation suffers almost no scrambling, which allows recording of in-cell NMR spectra. It requires only mg quantities of the individual amino acids, which cost only ∼1−10 € per sample depending on the amino acid (Table S1).

Investigating α-Syn at 310 K in Cells Using ^{13}Cα^{13}CO. First, we noticed in 2D ^{1}H−^{15}N HSQC recorded at 283 K that α-syn expressed in situ at ∼10 μM produced NMR signals similar to those observed in published studies, where recombinant purified α-syn had been delivered in human cells using electroporation.[22,23] The crosspeaks are those from a monomeric, disordered α-syn. We did not detect its N-terminal residues (residues 1−20) in live cells but crosspeaks of the N-ter acetylated form of α-syn reappeared in heated cell extracts (Figure 2a). Indeed, α-syn is heat stable (Figure S4),[49] and thus the peak disappearance in cells revealed interactions with heat-precipitable cellular components, among which chaperones Hsc70 and Hsp90 play a major role according to previous studies.[22,23]

However, α-syn's interactions with chaperones and lipid membranes are temperature dependent.[23,50−52] These can now

https://doi.org/10.1021/jacs.5c15061
J. Am. Chem. Soc. 2025, 147, 46259−46269

be studied at physiological pH and temperature in a residue-resolved fashion using $^{13}C\alpha$-^{13}CO experiments. As a test case, we recorded spectra of α-syn in the presence of large unilamellar vesicles (LUVs) made from pig brain polar lipids: we observed lower signal intensities revealing an interaction with the LUVs on the first 100 amino acids only at 310 K, and not at 283 K (Figure S5); this was thus only detectable using $^{13}C\alpha$-^{13}CO experiments and not using the classical $^{1}H-^{15}N$ HSQC. Moreover, these $^{13}C\alpha$-^{13}CO experiments were sufficiently sensitive and accurate to delineate clear differences in the binding modes of mutant forms of α-syn-A30P and F4A, which both have reduced affinities to lipid membranes (Figure S5).[22,53−55]

We sought to investigate this aspect at 310 K in $^{13}C-$K/F/L/V/Y-labeled cells expressing α-syn. First, the detected signals tallied with those of purified α-syn in terms of chemical shifts (Figures 2b, S6 and S7 shows the absence of leakage and the evolution of cell viability). However, most of the $^{13}C\alpha$-^{13}CO crosspeaks of α-syn in cells were attenuated. After normalization according to concentrations and isotopic incorporation levels, the profile of residue-resolved intensities showed features already observed in previous studies at 283 K: the 20 first residues were almost not detected, and the last 20 residues have attenuated intensities, all of which can be imputed to interactions with chaperones.[22,23] However, residues between positions 20 and 80 also had weak intensities in cells, which was not observed earlier at low temperature. Such signal losses show similitudes with those observed in the presence of LUVs at 310 K (Figures 2c and S5). To test this hypothesis, we performed the same experiments with stable-inducible cell lines expressing the weak lipid-binders mutants α-syn-F4A and the pathogenic α-syn-A30P. We observed intensity profiles similar to those of α-syn-WT, even though slightly higher intensities were observed between residues 20 and 80. This would be consistent with the existence of a non-negligible population of lipid-bound α-syn (Figure 2c).

Altogether, the in-cell spectra revealed the presence of a major population of disordered α-syn at 310 K, which might include a lipid-binding subpopulation. We are limited in our interpretation by S/N in our conditions at this magnetic field, which we discuss later.

Investigating Tau at 310 K in Cells Using $^{13}C\alpha$-^{13}CO Experiments. Then, we sought to apply our approach to other IDPs, and chose an emblematic long one, tau-2N4R (441 residues), whose role in so-called tauopathies calls for improved knowledge.[21] Because earlier assignments were obtained on shorter constructs or at pH 6.5 or less, we achieved a near-complete backbone assignment at pH 7 and 283 K using a 1.2 GHz spectrometer (BMRB code 52554). We transferred the $^{13}C\alpha$-^{13}CO assignment at 310 K using a temperature gradient (Figure S8).

Then, we recorded $^{13}C\alpha$-^{13}CO spectra—at 310 K and 700 MHz—of a stable-inducible cell line expressing tau-2N4R, which we labeled with $^{13}C-$F/I/L/R/V/Y. To obtain exploitable NMR signals, we had to supplement the culture medium with butyrate at 2 mM, which increases the doxycycline-induced expression by a factor 2 (Figure S1b). We observed only a few weak crosspeaks overlapping with those from the ∼150 N-terminal residues of purified tau (Figure 3a). At the opposite, other peaks were reproducibly missing, notably those from residues in the R1-R2-R3-R4 region (Figure 3b). This may reveal a population of tau that is free from any interaction in the N-terminal region, while the microtubule (MT) binding regions are either adopting ordered structures and/or transient interactions with cellular components. These regions are known to bind chaperones and MTs and also to be involved in aggregates found in patients with tauopathies.[21,56,57] To test the hypothesis of MTs binding, we supplemented tau-expressing HEK cells with colchicine at 20 μM during 24 h, leading to MTs disassembly and the progressive detachment of cells from the flask (Figure S9). In-cell spectra were highly similar to those of nontreated cells, showing only weak signals from the N-terminal residues, possibly until aa200. Hence, our results do not seem to reveal a dominant binding to MTs but fit better to tau-2N4R binding to lipid membranes, proline-binding proteins, chaperones, or being involved in liquid−liquid phase separation (LLPS).[56,58−61] Immuno-fluorescence microscopy did not reveal any aggregates or any condensates (Figure S10). Instead, tau was observed to be rather homogeneously dispersed in the cytosol and excluded from the nucleus, with only weak apparent colocalization with tubulin or membranes.

$^{13}C\alpha$-^{13}CO Acquisition at Higher Magnetic Fields. We verified that $^{13}C\alpha$-^{13}CO experiments can provide improved signal and resolution up to 1.2 GHz, which is the highest commercial magnetic field accessible. It was questionable because amide ^{13}CO have a large chemical shift anisotropy (CSA), which provokes T2 relaxation scaling with the square of the magnetic field.[62−64] This would come with broader and weaker signals at ultrahigh fields, counterbalancing the desired improvements of large magnets on the resolution and signal. Interestingly, we measured almost constant ^{13}CO line widths in Hz and peak intensities scaling with the probe sensitivity from 700 to 1200 MHz (Figure S11). This is in agreement with recent evaluations of ^{13}C-detected experiments on IDPs at 1.2 GHz.[65] It is consistent with the facts that (i) IDPs are weakly affected by CSA effects due to their high flexibility and (ii) ^{13}C-detection sensitivity scales well with the magnetic field even in watery and salty samples analyzed using a cryoprobe.[66] We had immediate access to a 700 MHz spectrometer equipped with a ^{13}C-detection optimized probe, which offered a much higher ^{13}C-sensitivity than the accessible 950 and 1200 MHz spectrometers equipped with ^{1}H-optimized probes. Using a ^{13}C-dedicated probe at 1.2 GHz should provide about twice the resolution and sensitivity of our 700 MHz spectrometer for $^{13}C\alpha$-^{13}CO experiments.

CONCLUSIONS

Our work aimed at establishing experimental conditions for in-cell NMR of IDPs closer to physiological conditions. The present set of methods proved to give access to residue-specific information on α-syn at intracellular concentrations of ∼10 μM and at 310 K. Even though intrinsically less sensitive than ^{1}H-detection, ^{13}C-detection permits one to approach such native concentrations. It has great advantages for in-cell analysis: ^{13}C-detection is much less affected by water signal and inhomogeneities in magnetic susceptibility than ^{1}H-detection.[67,68]

From a technical point of view, a few points can be highlighted. Leucine, valine, and isoleucine could be incorporated using their immediate ketoacids precursors, which are subject to a high transaminase activity, in agreement with recent reports.[45,47] This will permit ^{13}C-labeling at a reduced price in mammalian cells. At the opposite, some amino acids could be incorporated without any ^{15}N-scrambling, in agreement with other studies.[41−44] This should

https://doi.org/10.1021/jacs.5c15061
J. Am. Chem. Soc. 2025, 147, 46259−46269

enable residue-specific $^{13}C/^{15}N$-combined to ^{2}H-labeling schemes in mammalian cells, offering high sensitivity on folded proteins.[47,69]

From the biological point of view, we detected populations of α-syn and tau adopting disordered conformations in cells at 310 K. α-Syn appears to interact with cellular species on its N- and C-termini, in a similar fashion to that at 283 K. α-Syn also appears to experience supplementary binding, which were not observed at 283 K. Lipid membranes are the usual suspects in the case of α-syn, and we have shown that higher temperatures enable lipid-binding phenomena that did not occur at low temperatures, which we can characterize now using ^{13}C-detection. The present intensity profiles suggest the existence of non-negligible subpopulations binding transiently to lipid surfaces. This motivates further investigations at higher α-syn concentrations, higher magnetic fields, and in improved cellular models, which will allow better S/N and increased confidence in our interpretation.

Concerning tau, the treatment by colchicine revealed that the missing signals between residues 150 and 441 of tau were not, or were not only due to, microtubule binding. Tau interactome is profuse,[56,58−61,70,71] as are its functions and its detected post-translational modifications.[72] These are many possible reasons for signal losses, either related to interactions or to population heterogeneity. It would be difficult to interpret immediately the profiles observed here. To identify important players responsible for the observed weak signals, a number of in vitro titrations with various tau-binders would be necessary, as well as many silencing experiments of these binding partners of tau. It might not be worth conducting such a research program with the HEK cell lines used here. Future studies on more advanced cellular models will make it more interesting. Hence, these early analyses motivate further investigations and will most probably require the complementary use of solution and solid-state NMR.

Future studies will examine improved cellular models: HEK cells are convenient to manipulate, but neuronal cells would be more relevant to studying α-syn/tau-linked neurodegeneration. Biological interpretation of the present results must be cautious, given the progressive loss of cell viability generated by rudimentary experimental conditions, which can be improved. The use of a flow-probe bioreactor will be instrumental to achieve a longitudinal monitoring in steady, wealthy conditions.[10] This requires the trapping of cells in gels, which decreases the number of detected molecules in the NMR probe, hence their NMR signal. Using our $^{13}C\alpha$-^{13}CO approach, an intracellular concentration of 10 μM is a lower limit to obtain exploitable signals in a few hours at 700 MHz. Higher fields will help solving this sensitivity issue: the $^{13}C\alpha$-^{13}CO experiment yields S/N scaling with the field, in contrast to ^{1}H-detected experiments.[66] Higher cellular concentrations of α-syn, i.e., ∼20−30 μM, would yield much better spectra, while remaining in the range of native concentrations for α-syn. This can be reached by multiple insertions of the GOI.[73−76] This strategy, followed by clonal selection, allows homogeneous clonal cell lines with selected levels of inducible expression to be obtained, as recently demonstrated by Trantirek and co-workers.[76] Their approach will be most often better suited to in-cell NMR studies than the single-locus insertion used here, even though it can generate some genetic disorders that require additional controls.

Even though recent methods have been developed to predict isolated IDPs conformational ensembles,[16,77] experimental information on the effects of cellular conditions is still needed to understand how IDPs behave, function, and eventually misfold. We presented here a set of methods that will enable such experimental studies, providing residue-specific in-cell characterizations of IDPs at physiological concentrations and temperatures. Extensive interactions with cellular entities may hinder this approach, as revealed by the high concentrations of tau required for its detection. Further research is needed to determine the frequency of such a phenomenon.

MATERIAL AND METHODS

Generation of Inducible Stable Cell Lines. α-Syn and tau cDNAs were codon-optimized for expression in human cells and synthesized by Genscript, before being cloned into a pcDNA5/FRT/TO/EGFP vector (kind gift from A.M. Tassin) at the *Bam*HI/NotI restriction sites. The coding sequence for EGFP was removed from the parental plasmid by mutation (Genscript), and the later plasmid containing the genes coding for α-Syn-F4A, α-Syn-A30P and α-Syn-aa1−103 was also obtained by single point mutation (Genscript). The pOG44 Flp-Recombinase Expression Vector was purchased from Invitrogen (ref V600520).

Parental Flp-In T-Rex HEK 293 cells were a kind gift from A.M. Tassin (Institute for Integrative Biology of the Cell, Gif-sur-Yvette, France). These were cultivated in Dulbecco's modified Eagle's medium (StableCell DMEM-high glucose-Glutamax, Sigma, ref D0819) supplemented with 10% (v/v) fetal bovine serum (FBS, Gibco, ref 10270-106) (abbrev. below: DMEM-FBS), 100 U/mL penicillin, and 10 μg/mL streptomycin (Sigma, ref P4333), 10 μg/mL blasticidin (Invivogen, Cat# ant-bl-1) and 100 μg/mL zeocin (Zeocin Selection Reagent, Gibco, ref R25001).

For generating the stable cell lines, the parental Flp-In T-Rex HEK 293 cells were seeded in a 6-well plate (3.5 cm diameter) at a density of 300,000 cells per well and 24 h prior transfection. Cells were then washed with phosphate-buffered saline (PBS, Sigma, D8537) and incubated 8 h with a 1:1:2 ratio (w/w) of pcDNA5-(α-Syn/tau):pOG44:PEI in 2 mL of DMEM (using 4 μg of plasmid). The transfection reagent was PEI MAX (Transfection grade linear polyethyleiminine, MW 40,000, Polysciences ref 24765-1). Cells were later washed and maintained in DMEM-FBS during 24 h. Cells that integrated the α-syn or tau cDNA were selected in DMEM-FBS supplemented with 200 μg/mL hygromycin, 100 U/mL penicillin, and 10 μg/mL streptomycin (Sigma, ref P4333), 10 μg/mL blasticidin (Invivogen, Cat# ant-bl-1) and 100 μg/mL zeocin (Zeocin Selection Reagent, Gibco, ref R25001). The medium was refreshed every day in the first 2 days, and every 5 days once, the nontransformed cells detached under hygromycin pressure. Colonies were detected after 3 to 4 weeks. These were trypsinized and progressively transferred into larger culture plates to reach about 150 million cells (i.e., passage ∼ 20). These were finally trypsinized, washed, and resuspended in FBS supplemented with 10% (v/v) DMSO (Sigma-Aldrich, ref D8418). Aliquots of 5−10 million cells were slowly frozen at −70 °C using a freezing container (Corning CoolCell LX) and stored in liquid nitrogen. They were later thawed and cultured in DMEM-FBS supplemented with 100 μg/mL hygromycin, 100 U/mL penicillin,10 μg/mL streptomycin (Sigma, ref P4333), 5 μg/mL blasticidin (Invivogen, Cat# ant-bl-1) and 50 μg/mL zeocin (Zeocin Selection Reagent, Gibco, ref R25001).

All cells were grown at 37 °C in a humidified atmosphere at 5% CO_2. Cell lines were tested for mycoplasma contaminations and were found mycoplasma-free.

In-Cell NMR Sample. To generate in-cell NMR samples, cells from an established Flp-In T-Rex HEK 293 cell line were grown at 70% confluence in a 300 cm^2 tissue culture flask. Four hours before induction, cells were washed with PBS and the medium was replaced with homemade DMEM (according to the composition of DMEM-high glucose-Glutamax, Sigma, ref D0819), supplemented with

https://doi.org/10.1021/jacs.5c15061
J. Am. Chem. Soc. 2025, 147, 46259−46269

dialyzed FBS (Gibco, ref A3382001), Glutamax (Gibco, ref 35050-038), and with the desired labeled amino acids (see Table S1). When using Leu, Val, and Ile precursors, i.e., [1,2-$^{13}C_2$]-α-ketoisocaproate, [u-^{13}C]-α-ketoisovalerate, and [u-^{13}C]-2-keto-3-methyl pentanoate, respectively, we supplemented them to the medium at the concentrations indicated for their final amino acid counterparts in a DMEM (Table S1). For Gly labeling, we removed Ser from the recipe and supplemented the medium with 4x the normal concentration of Gly (i.e., 120 mg/L).

Cells were induced with doxycycline at 10 ng/mL, which we determined to be sufficient for maximal expression rates (Figure S1) (Sigma D9891). After 44−48 h of protein expression in these conditions, cells were detached using trypsin-EDTA (Sigma, ref T4174), washed once with DMEM-FBS and then twice in PBS, resuspended in 450 μL of fresh DMEM-FBS supplemented with D_2O at 10% v/v, and pelleted into a 5 mm (diameter) advanced Shigemi NMR.

Purification of Induced α-Syn from In-Cell NMR Samples and Acid Hydrolysis. Recombinant α-syn was purified from in-cell NMR samples produced with [1,2-$^{13}C_2$]-α-ketoisocaproate, [u-^{13}C]-α-ketoisovalerate, and [u-^{13}C^{15}N]-Lys/Phe/Tyr according to the protocol described in the previous paragraph. Two 150 cm^2 plates were necessary to achieve proper purification from the established Flp-In T-Rex HEK 293 cell line. The purification was achieved using a classical approach, as described in previous publications.[22] In brief, we carried out an initial boiling step of the cell extract, a nucleic acid precipitation by streptomycin at 10 g/L, α-synuclein precipitation by NH_4−SO_4 at 36% w/v, and an anion-exchange chromatography followed by a final size-exclusion chromatography in ammonium acetate at 50 mM, pH = 7. The samples were finally freeze-dried overnight. This yielded about 1 nmol of pure α-synuclein.

Then, the hydrolysis of the α-synuclein samples was performed according to the vapor phase HCl hydrolysis method: 10 μL of the protein resuspended in water were transferred into clean borosilicate tubes (in duplicates or triplicates). Tubes were placed in a 40 mL screw cap bottle (equipped with a slide valve) and then vacuum-dried using a Waters Pico-Tag workstation. 200 μL of 6 N HCl Sequanal grade (constant boiling) (Thermo Fisher Pierce) was then added into the screw cap bottle. This bottle was flushed 3 times by argon and on the last vacuum step was closed by the slide valve. The bottle was placed in an oven heated at 110 °C for 18 h. After the hydrolysis step, HCl vapor was evacuated from the bottle vacuum-dried using the Waters Pico-Tag workstation. Hydrolyzed peptides in borosilicate tubes were resuspended in an LC-MS solvent before analyses.

Analysis of Amino Acid Residues by Liquid Chromatography Coupled to High Resolution Mass Spectrometry (LC-MS). LC-MS experiments were performed by using a Dionex Ultimate chromatographic system (Thermo Fisher Scientific) coupled to a QExactive (Orbitrap) mass spectrometer (Thermo Fisher Scientific) fitted with an electrospray ion source. The mass spectrometer was externally calibrated before each analysis using the manufacturer's predefined methods and provided a recommended calibration mixture.

Chromatographic separation was performed on an Acquity UPLC HSS PFP 1.8 μm, 2.1 × 100 mm (Waters) at 30 °C. The chromatographic system was equipped with an online prefilter (Thermo Fisher Scientifics). Mobile phases were 100% water (A) and 100% acetonitrile (B), both of which contained 0.1% formic acid. Chromatographic elution was achieved at a flow rate of 250 mL/min. After sample injection (20 mL), elution started with an isocratic step of 2 min at 0% phase B, followed by a linear gradient from 0 to 100% phase B in 18 min. These proportions were kept constant for 4 min before returning to 0% of phase B and letting the system equilibrate for 6 min. The column effluent was directly introduced into the electrospray source of the mass spectrometer, and analyses were performed in positive ion mode.

Source parameters were as follows: capillary voltage set at 3 kV; capillary temperature at 300 °C; sheath and auxiliary gas (nitrogen) flow rates at 50 and 25 arbitrary units, respectively; and mass resolution power of the analyzer set at 140,000 at m/z 200 (full width at half-maximum, fwhm) for singly charged ions. The acquisition was achieved from m/z 50 to 250 in the positive ionization mode during all of the acquisition. Under these conditions, we achieved a good chromatographic separation and detection (with an average mass accuracy better than 3 ppm) of the targeted amino acids under their $[M + H]^+$ form. These species were readily identified and quantified by the isotope dilution method using ^{13}C, ^{15}N-labeled homologues. Corresponding extracted ion chromatograms were generated and resulting peaks were integrated using the Trace Finder software (version 4.1, Thermo Fisher Scientific) according to the RT and $[M + H]^+$ values listed in the Table S5.

Verification of the Absence of Protein Leakage during In-Cell NMR Spectra Acquisition. Protein leakage was controlled after in-cell NMR acquisition by recording ^{13}Cα-^{13}CO spectra of the sample supernatant, which was obtained as follows: cells were resuspended in the 450 μL of medium in excess in the NMR tube, transferred in a 1.5 mL tube, and pelleted by centrifugation at 100 g during 3 min; the resulting supernatant was analyzed using the same tube and NMR parameters than in-cell samples.

Production of Cell Extracts for NMR Analysis. Lysis of HEK cells after in-cell NMR was performed by sonication on ice using a Q700 sonicator (Qsonica). A wet pellet of cells (∼300 μL) was sonicated on ice during 3 min using 5 s ON/25 s OFF cycles of sonication (40% amplitude) in 400 μL of PBS (Sigma ref D1408), supplemented with protease inhibitors (cOmplete EDTA-free, Sigma ref 05056489001) and DTT at 2 mM. The cell extracts were cleared using centrifugation at 15,000 g for 10 min at 4 °C. Folded proteins were precipitated by thermal denaturation at 95 °C for 3 min. The final cell extracts were obtained using centrifugation at 15,000 g for 10 min at 4 °C. NMR spectra were acquired in the supernatant.

Western Blot and Quantification of Intracellular Concentrations. The protein expression quantification was performed on HEK cells after 48h in labeled DMEM with and without induction of protein expression. The cells were diluted to 25 million cells/mL and lysed in a RIPA lysis buffer (20 mM Tris, 150 mM NaCl, 1% (v/v) Nonidet P40 (USB), 1% (v/v) sodium deoxycholate (Sigma-Aldrich ref D6750), 0,1% (v/v) SDS), supplemented with protease inhibitor (cOmplete, EDTA-free, Sigma ref 05056489001) for 20 min on ice, followed by sonication on ice (5s, 40% amplitude using Q700 sonicator Qsonica). Aliquots containing about 150,000 lysed cells were loaded per well for SDS-PAGE analysis (15% acrylamide). To quantify the concentration of α-Syn in these cells, a dilution series of 11−44 ng of purified α-syn (expressed recombinantly in bacteria, see above) was also loaded on the gels. Assuming a cellular volume of 1 pL (average diameter 13 ± 2 μm, Biorad TC20 Automated Cell Counter), the corresponding intracellular concentrations of the latter series were 5, 10, 15, and 20 μM.

After SDS-PAGE migration, proteins were transferred onto nitrocellulose membranes (GE Healthcare Life Science), using Trans-Blot turbo (Biorad). After blocking for 1h in 5% (w/v) skim milk (Sigma, ref 70166) in TBST (0.1% (v/v) Tween-20, 20 mM Tris, 150 mM NaCl, pH 7.5), membranes were probed with the anti-α-syn antibody ab-138501 (Abcam, 1:10,000 dilution), antitau HT-7 and T46 (Invitrogen, ref MN1000 & 13-6400,1:1500 and 1:1000 dilutions, respectively), and anti-β-actine antibody A1978 (Sigma, 1:10,000 dilution) for 30 min to 1h at room temperature. Secondary antibodies were HRP-conjugated antirabbit or antimouse (Thermo Scientific, ref 31460 and 31430, dilution 1:10,000) and were incubated during 45 min with the membranes. Membranes were developed using clarity Western ECL Substrate (Bio-Rad). Luminescence signals were detected on a Bio-Rad ChemiDoc imaging system and quantified with Image Lab 5.1 (Bio-Rad).

NMR Acquisition and Processing of 2D Reference and In-Cell Spectra. In-cell NMR spectra were recorded using 700 MHz Bruker Avance Neo spectrometers, equipped with cryogenically cooled triple resonance probes, namely, ^{1}H{^{13}C/^{15}N} TCI and ^{13}C{^{1}H/^{15}N} TXO probes for spectra at 10 °C (^{1}H-detection) and 37 °C (^{13}C-detection), respectively. We used 5 mm Shigemi (for ^{1}H-detection) or 5 mm Shigemi advanced (for ^{13}C-detection) NMR tubes without a plunger. All spectra were acquired and processed with

https://doi.org/10.1021/jacs.5c15061
J. Am. Chem. Soc. 2025, 147, 46259−46269

Topspin 4. The TCI probe is from 2006 and its sensitivity was determined to be S/N = 7260 for ^{1}H 0.1% ethylbenzene when delivered. The 700 MHz-TXO probe is from 2020 and its sensitivity was determined to be S/N = 3400 for ^{13}C ASTM when delivered.

"Cell-extract" and "in-cell" spectra were recorded with exactly the same parameters for the "induced" and "non-induced" samples. This permitted the later subtraction of the raw FIDs to remove the signal from the cellular background, which is due to integration of the isotope-labeled amino acids in the proteome. The background broad signal from isotope-labeled peptides proved to be independent of the expression of the protein of interest and thus can be removed using FID subtraction. However, the strong, sharper signals from abundant metabolites (e.g., amino acids) are often not canceled perfectly. Also, because the number of cells in the tube was not always exactly the same, we had to apply a multiplication factor to the "non-induced" spectra to remove the cellular background signal. This factor varied between 0.8 and 1.2, which we fixed based on the best possible canceling of the baseline in the final spectrum. The subtraction of the "non-induced spectrum" was not necessary for ^{13}C-Phe/^{13}C-Tyr, the cellular background signal being negligible. The addition and subtraction of raw FIDs were performed by using Topspin 4. The peak intensity analysis was carried out using ccpNMR 3.1.1.[78]

All $^{13}C\alpha^{13}CO$ correlation spectra were acquired using the (^{1}H-flip*)-$^{13}C\alpha^{13}CO$-LB pulse sequence[34] at 37 °C. The interscan delay was 0.2 s, which yields the best signal-to-noise ratio per unit of time for disordered proteins, according to our previous quantifications.[34]

The 950 MHz-TCI probe had a S/N of 1710 for ^{13}C ASTM (40% dioxane in C_6D_6, ASTM) when delivered. The 1200 MHz-TCI-3 mm probe had a S/N = 805 for ^{13}C ASTM when delivered.

Preparation of Lipid Vesicles. Pig brain polar lipid extracts were purchased from Avanti. Lipid stock solutions were mixed in appropriate molar ratios in chloroform and lyophilized overnight. The dried lipids were solubilized in PBS (20 mM phosphate and 150 mM NaCl), pH 7.2. SUVs and LUVs were prepared by sonication (2 × 20 min, 30% amplitude, Vibracell 75042 BIOBLOCK SC) on ice. LUVs were obtained in the case of the pig brain polar lipid extract solubilized in PBS, while SUVs were obtained in many other buffers. We obtained SUVs from pig brain polar lipid extract solubilized and sonicated in hepes 20 mM and NaCl 50 mM, pH 7.2. Then, vesicles were centrifugated at 14,000 *g* to remove any metal residue from the sonicator probe. The vesicle size was determined by dynamic light scattering (DLS) (Nano series, Malvern).

■ ASSOCIATED CONTENT

Supporting Information

The Supporting Information is available free of charge at https://pubs.acs.org/doi/10.1021/jacs.5c15061.

Methods for recombinant production in *E. coli* and purification; further details on NMR spectra acquisition and processing parameters; NMR pulse sequence; Tables S1−S5: information on labeled amino acids, their scrambling and their incorporation rates; and Figures S1−S10: expression tests, full-window NMR spectra of failing and successful specific labeling assays of leakage tests, Western blot analysis of cell extracts, NMR analysis of lipid vesicle binding, and line width analysis in function of magnetic fields (PDF)

■ AUTHOR INFORMATION

Corresponding Author

Francois-Xavier Theillet − *Université Paris-Saclay, CEA, CNRS, Institute for Integrative Biology of the Cell (I2BC), 91198 Gif-sur-Yvette, France; Université Paris Cité, CNRS, CiTCoM, F-75006 Paris, France;* orcid.org/0000-0002-3264-210X; Email: francois-xavier.theillet@cnrs.fr

Authors

Hélène Chérot − *Université Paris-Saclay, CEA, CNRS, Institute for Integrative Biology of the Cell (I2BC), 91198 Gif-sur-Yvette, France*

Théophile Pred'homme − *Université Paris Cité, CNRS, CiTCoM, F-75006 Paris, France*

Robert Thai − *Université Paris-Saclay, CEA, INRAE, Médicaments et Technologies pour la Santé (MTS), SIMoS, 91191 Gif-sur-Yvette, France*

Frédéric Théodoro − *Université Paris-Saclay, CEA, INRAE, Département Médicaments et Technologies pour la Santé (DMTS), MetaboHUB, 91191 Gif-sur-Yvette, France*

Florence Castelli − *Université Paris-Saclay, CEA, INRAE, Département Médicaments et Technologies pour la Santé (DMTS), MetaboHUB, 91191 Gif-sur-Yvette, France*

Complete contact information is available at: https://pubs.acs.org/10.1021/jacs.5c15061

Author Contributions

The manuscript was written through contributions of all authors. All authors have given approval to the final version of the manuscript.

Notes

The authors declare no competing financial interest.

■ ACKNOWLEDGMENTS

This article is adapted for a good part from a thesis, see https://theses.fr/2024UPASQ030. This work was supported by the CNRS and the CEA-Saclay (CEA/PSAC/DPRS/BE/TG/2021-410), by the French Infrastructure for Integrated Structural Biology (https://frisbi.eu/, grant number ANR-10-INSB-05-01, Acronym FRISBI) and by the French National Research Agency (ANR; research grants ANR-14-ACHN-0015 and ANR-20-CE92-0013). Financial support from the IR INFRANALYTICS FR2054 for conducting the research is gratefully acknowledged, and we value the commitment and expertise of X. Trivelli and F.-X. Cantrelle. We acknowledge Virginie Mignon and Bruno Saubaméa from the PICMO facility (US25 Inserm, UAR3612 CNRS, Faculty of Pharmacy of Paris, University Paris Cité, Paris, France) for immunostaining experiments and confocal imaging. We thank also Guillaume Sarrabayrouse from the Multidimensional Cellular Analysis facility from Faculté de Pharmacie de Paris (Université Paris Cité, CNRS, Inserm, PMIM, F-75006 Paris, France) for his assistance with the flow cytometer, and his substantial help in cell-cycle analysis.

■ ABBREVIATIONS

α-syn, α-synuclein; doxy., doxycycline; GOI, gene of interest; IDRs/IDPs, intrinsically disordered (regions of) proteins; MS, mass spectrometry; MT, microtubule; NMR, nuclear magnetic resonance; PBS, phosphate-buffered saline

■ REFERENCES

(1) Theillet, F.-X. In-Cell Structural Biology by NMR: The Benefits of the Atomic Scale. *Chem. Rev.* **2022**, *122* (10), 9497−9570.

(2) Nogales, E.; Mahamid, J. Bridging Structural and Cell Biology with Cryo-Electron Microscopy. *Nature* **2024**, *628* (8006), 47−56.

(3) Goldfarb, D. Exploring Protein Conformations in Vitro and in Cell with EPR Distance Measurements. *Curr. Opin. Struct. Biol.* **2022**, *75*, No. 102398.

(4) Yu, M.; Heidari, M.; Mikhaleva, S.; Tan, P. S.; Mingu, S.; Ruan, H.; Reinkemeier, C. D.; Obarska-Kosinska, A.; Siggel, M.; Beck, M.;

Hummer, G.; Lemke, E. A. Visualizing the Disordered Nuclear Transport Machinery in Situ. *Nature* **2023**, *617* (7959), 162−169.
(5) Schuler, B.; König, I.; Soranno, A.; Nettels, D.; et al. Impact of In-cell and In-vitro Crowding on the Conformations and Dynamics of an Intrinsically Disordered Protein. *Angew. Chem., Int. Ed.* **2021**, *60*, 10724.
(6) Plitzko, J. M.; Schuler, B.; Selenko, P. Structural Biology Outside the Box-inside the Cell. *Curr. Opin. Struct. Biol.* **2017**, *46*, 110−121.
(7) Zhang, Z.; Zhao, Q.; Gong, Z.; Du, R.; Liu, M.; Zhang, Y.; Zhang, L.; Li, C. Progress, Challenges and Opportunities of NMR and XL-MS for Cellular Structural Biology. *JACS Au* **2024**, *4* (2), 369−383.
(8) McCafferty, C. L.; Klumpe, S.; Amaro, R. E.; Kukulski, W.; Collinson, L.; Engel, B. D. Integrating Cellular Electron Microscopy with Multimodal Data to Explore Biology across Space and Time. *Cell* **2024**, *187* (3), 563−584.
(9) Beck, M.; Covino, R.; Hänelt, I.; Müller-McNicoll, M. Understanding the Cell: Future Views of Structural Biology. *Cell* **2024**, *187* (3), 545−562.
(10) Luchinat, E.; Cremonini, M.; Banci, L. Radio Signals from Live Cells: The Coming of Age of In-Cell Solution NMR. *Chem. Rev.* **2022**, *122* (10), 9267−9306.
(11) Dyson, H. J.; Wright, P. E. NMR Illuminates Intrinsic Disorder. *Curr. Opin. Struct. Biol.* **2021**, *70*, 44−52.
(12) Camacho-Zarco, A. R.; Schnapka, V.; Guseva, S.; Abyzov, A.; Adamski, W.; Milles, S.; Jensen, M. R.; Zidek, L.; Salvi, N.; Blackledge, M. NMR Provides Unique Insight into the Functional Dynamics and Interactions of Intrinsically Disordered Proteins. *Chem. Rev.* **2022**, *122* (10), 9331−9356.
(13) Lemke, E. A.; Babu, M. M.; Kriwacki, R. W.; Mittag, T.; Pappu, R. V.; Wright, P. E.; Forman-Kay, J. D. Intrinsic Disorder: A Term to Define the Specific Physicochemical Characteristic of Protein Conformational Heterogeneity. *Mol. Cell* **2024**, *84* (7), 1188−1190.
(14) Aspromonte, M. C.; Nugnes, M. V.; Quaglia, F.; Bouharoua, A.; DisProt Consortium; Sagris, V.; Promponas, V. J.; Chasapi, A.; Fichó, E.; Balatti, G. E.; Parisi, G.; Buitrón, M. G.; Erdos, G.; Pajkos, M.; Dosztányi, Z.; Dobson, L.; Conte, A. D.; Clementel, D.; Salladini, E.; Leonardi, E.; Kordevani, F.; Ghafouri, H.; Ku, L. G. T.; Monzon, A. M.; Ferrari, C.; Kálmán, Z.; Nilsson, J. F.; Santos, J.; Pintado-Grima, C.; Ventura, S.; Ács, V.; Pancsa, R.; Kulik, M. G.; Andrade-Navarro, M. A.; Pereira, P. J. B.; Longhi, S.; Mercier, P. L.; Bergier, J.; Tompa, P.; Lazar, T.; Tosatto, S. C. E.; Piovesan, D. DisProt in 2024: Improving Function Annotation of Intrinsically Disordered Proteins. *Nucleic Acids Res.* **2024**, *52* (D1), D434−D441.
(15) Holehouse, A. S.; Kragelund, B. B. The Molecular Basis for Cellular Function of Intrinsically Disordered Protein Regions. *Nat. Rev. Mol. Cell Biol.* **2024**, *25* (3), 187−211.
(16) Tesei, G.; Trolle, A. I.; Jonsson, N.; Betz, J.; Knudsen, F. E.; Pesce, F.; Johansson, K. E.; Lindorff-Larsen, K. Conformational Ensembles of the Human Intrinsically Disordered Proteome. *Nature* **2024**, *626*, 897−904.
(17) Theillet, F.-X.; Binolfi, A.; Frembgen-Kesner, T.; Hingorani, K.; Sarkar, M.; Kyne, C.; Li, C.; Crowley, P. B.; Gierasch, L.; Pielak, G. J.; Elcock, A. H.; Gershenson, A.; Selenko, P. Physicochemical Properties of Cells and Their Effects on Intrinsically Disordered Proteins (IDPs). *Chem. Rev.* **2014**, *114* (13), 6661−6714.
(18) Moses, D.; Ginell, G. M.; Holehouse, A. S.; Sukenik, S. Intrinsically Disordered Regions Are Poised to Act as Sensors of Cellular Chemistry. *Trends Biochem. Sci.* **2023**, *48* (12), 1019−1034.
(19) Oliveira, L. M. A.; Gasser, T.; Edwards, R.; Zweckstetter, M.; Melki, R.; Stefanis, L.; Lashuel, H. A.; Sulzer, D.; Vekrellis, K.; Halliday, G. M.; Tomlinson, J. J.; Schlossmacher, M.; Jensen, P. H.; Schulze-Hentrich, J.; Riess, O.; Hirst, W. D.; El-Agnaf, O.; Mollenhauer, B.; Lansbury, P.; Outeiro, T. F. Alpha-Synuclein Research: Defining Strategic Moves in the Battle against Parkinson's Disease. *Npj Park Dis* **2021**, *7* (1), 65.
(20) Simuni, T.; Chahine, L. M.; Poston, K.; Brumm, M.; Buracchio, T.; Campbell, M.; Chowdhury, S.; Coffey, C.; Concha-Marambio, L.; Dam, T.; DiBiaso, P.; Foroud, T.; Frasier, M.; Gochanour, C.; Jennings, D.; Kieburtz, K.; Kopil, C. M.; Merchant, K.; Mollenhauer, B.; Montine, T.; Nudelman, K.; Pagano, G.; Seibyl, J.; Sherer, T.; Singleton, A.; Stephenson, D.; Stern, M.; Soto, C.; Tanner, C. M.; Tolosa, E.; Weintraub, D.; Xiao, Y.; Siderowf, A.; Dunn, B.; Marek, K. A Biological Definition of Neuronal α-Synuclein Disease: Towards an Integrated Staging System for Research. *Lancet Neurol.* **2024**, *23* (2), 178−190.
(21) Creekmore, B. C.; Watanabe, R.; Lee, E. B. Neurodegenerative Disease Tauopathies. *Annu. Rev. Pathol. Mech. Dis.* **2024**, *19* (1), 345−370.
(22) Theillet, F.-X.; Binolfi, A.; Bekei, B.; Martorana, A.; Rose, H. M.; Stuiver, M.; Verzini, S.; Lorenz, D.; van Rossum, M.; Goldfarb, D.; Selenko, P. Structural Disorder of Monomeric α-Synuclein Persists in Mammalian Cells. *Nature* **2016**, *530* (7588), 45−50.
(23) Burmann, B. M.; Gerez, J. A.; Matečko-Burmann, I.; Campioni, S.; Kumari, P.; Ghosh, D.; Mazur, A.; Aspholm, E. E.; Šulskis, D.; Wawrzyniuk, M.; Bock, T.; Schmidt, A.; Rüdiger, S. G. D.; Riek, R.; Hiller, S. Regulation of α-Synuclein by Chaperones in Mammalian Cells. *Nature* **2020**, *577* (7788), 127−132.
(24) Zhang, S.; Wang, C.; Lu, J.; Ma, X.; Liu, Z.; Li, D.; Liu, Z.; Liu, C. In-Cell NMR Study of Tau and MARK2 Phosphorylated Tau. *Int. J. Mol. Sci.* **2019**, *20* (1), 90.
(25) Hsu, S.-T. D.; Bertoncini, C. W.; Dobson, C. M. Use of Protonless NMR Spectroscopy To Alleviate the Loss of Information Resulting from Exchange-Broadening. *J. Am. Chem. Soc.* **2009**, *131* (21), 7222−7223.
(26) Kim, S.; Wu, K.-P.; Baum, J. Fast Hydrogen Exchange Affects ^{15}N Relaxation Measurements in Intrinsically Disordered Proteins. *J. Biomol. NMR* **2013**, *55* (3), 249−256.
(27) Yuwen, T.; Skrynnikov, N. R. CP-HISQC: A Better Version of HSQC Experiment for Intrinsically Disordered Proteins under Physiological Conditions. *J. Biomol NMR* **2014**, *58* (3), 175−192.
(28) Bai, Y.; Milne, J. S.; Mayne, L.; Englander, S. W. Primary Structure Effects on Peptide Group Hydrogen Exchange. *Proteins* **1993**, *17* (1), 75−86.
(29) Wuttke, R.; Hofmann, H.; Nettels, D.; Borgia, M. B.; Mittal, J.; Best, R. B.; Schuler, B. Temperature-Dependent Solvation Modulates the Dimensions of Disordered Proteins. *Proc. Natl. Acad. Sci. U.S.A.* **2014**, *111* (14), 5213−5218.
(30) Pesce, F.; Lindorff-Larsen, K. Combining Experiments and Simulations to Examine the Temperature-Dependent Behavior of a Disordered Protein. *J. Phys. Chem. B* **2023**, *127* (28), 6277−6286.
(31) Emenecker, R. J.; Holehouse, A. S.; Strader, L. C. Biological Phase Separation and Biomolecular Condensates in Plants. *Annu. Rev. Plant Biol.* **2021**, *72* (1), 17−46.
(32) Lopez, J.; Schneider, R.; Cantrelle, F.-X.; Huvent, I.; Lippens, G. Studying Intrinsically Disordered Proteins under True In Vivo Conditions by Combined Cross-Polarization and Carbonyl-Detection NMR Spectroscopy. *Angew. Chem., Int. Ed.* **2016**, *128* (26), 7544−7548.
(33) Bodor, A.; Haller, J. D.; Bouguechtouli, C.; Theillet, F.-X.; Nyitray, L.; Luy, B. Power of Pure Shift HαCα Correlations: A Way to Characterize Biomolecules under Physiological Conditions. *Anal. Chem.* **2020**, *92* (18), 12423−12428.
(34) Alik, A.; Bouguechtouli, C.; Julien, M.; Bermel, W.; Ghouil, R.; Zinn-Justin, S.; Theillet, F.-X. Sensitivity-Enhanced 13C-NMR Spectroscopy for Monitoring Multisite Phosphorylation at Physiological Temperature and pH. *Angew. Chem., Int. Ed.* **2020**, *59* (26), 10411−10415.
(35) Felli, I. C.; Pierattelli, R. ^{13} C Direct Detected NMR for Challenging Systems. *Chem. Rev.* **2022**, *122* (10), 9468−9496.
(36) Dominguez-Meijide, A.; Parrales, V.; Vasili, E.; González-Lizárraga, F.; König, A.; Lázaro, D. F.; Lannuzel, A.; Haik, S.; Del Bel, E.; Chehín, R.; Raisman-Vozari, R.; Michel, P. P.; Bizat, N.; Outeiro, T. F. Doxycycline Inhibits α-Synuclein-Associated Pathologies in Vitro and in Vivo. *Neurobiol. Dis.* **2021**, *151*, No. 105256.
(37) Wilhelm, B. G.; Mandad, S.; Truckenbrodt, S.; Kröhnert, K.; Schäfer, C.; Rammner, B.; Koo, S. J.; Claßen, G. A.; Krauss, M.; Haucke, V.; Urlaub, H.; Rizzoli, S. O. Composition of Isolated

https://doi.org/10.1021/jacs.5c15061
J. Am. Chem. Soc. 2025, 147, 46259−46269

Synaptic Boutons Reveals the Amounts of Vesicle Trafficking Proteins. *Nature* **2014**, *344* (6187), 1023−1028.
(38) Kanaan, N. M.; Grabinski, T. Neuronal and Glial Distribution of Tau Protein in the Adult Rat and Monkey. *Front. Mol. Neurosci.* **2021**, *14*, No. 607303.
(39) Huang, Q.; Szklarczyk, D.; Wang, M.; Simonovic, M.; Von Mering, C. PaxDb 5.0: Curated Protein Quantification Data Suggests Adaptive Proteome Changes in Yeasts. *Molecular & Cellular Proteomics* **2023**, *22* (10), No. 100640.
(40) Chen, X.; Wei, S.; Ji, Y.; Guo, X.; Yang, F. Quantitative Proteomics Using SILAC: Principles, Applications, and Developments. *Proteomics* **2015**, *15* (18), 3175−3192.
(41) Banci, L.; Barbieri, L.; Bertini, I.; Luchinat, E.; Secci, E.; Zhao, Y.; Aricescu, A. R. Atomic-Resolution Monitoring of Protein Maturation in Live Human Cells by NMR. *Nat. Chem. Biol.* **2013**, *9* (5), 297−299.
(42) Lee, K.; Lee, J. H. Stable Isotope Labeling of Proteins in Mammalian Cells. *J. Kor. Magn. Reson. Soc.* **2020**, *24* (3), 77−85.
(43) Luchinat, E.; Barbieri, L.; Cremonini, M.; Pennestri, M.; Nocentini, A.; Supuran, C. T.; Banci, L. Determination of Intracellular Protein−Ligand Binding Affinity by Competition Binding in-Cell NMR. *Acta Crystallogr. D Struct Biol.* **2021**, *77* (10), 1270−1281.
(44) Subedi, G. P.; Roberts, E. T.; Davis, A. R.; Kremer, P. G.; Amster, I. J.; Barb, A. W. A Comprehensive Assessment of Selective Amino Acid 15N-Labeling in Human Embryonic Kidney 293 Cells for NMR Spectroscopy. *J. Biomol NMR* **2024**, *78*, 125−132.
(45) Rößler, P.; Ruckstuhl, M.; Löbbert, A.; Stühlinger, T.; Franchini, L. R.; Tsai, C.-J.; Lichtenecker, R.; Shrestha, B.; Rüdisser, S. H.; Konrat, R.; Schertler, G. F. X.; Gossert, A. D. Human Cells for Human Proteins: Isotope Labeling in Mammalian Cells for Functional NMR Studies of Disease-Relevant Proteins. *bioRxiv* **2024**, No. 588766.
(46) Mallis, R. J.; Lee, J. J.; Berg, A. V. den; Brazin, K. N.; Viennet, T.; Zmuda, J.; Cross, M.; Radeva, D.; Rodriguez-Mias, R.; Villén, J.; Gelev, V.; Reinherz, E. L.; Arthanari, H. Efficient and Economic Protein Labeling for NMR in Mammalian Expression Systems: Application to a preT-cell and T-cell Receptor Protein. *Protein Sci.* **2024**, *33* (4), No. e4950.
(47) Rosati, M.; Barbieri, L.; Hlavac, M.; Kratzwald, S.; Lichtenecker, R. J.; Konrat, R.; Luchinat, E.; Banci, L. Towards Cost-Effective Side-Chain Isotope Labelling of Proteins Expressed in Human Cells. *J. Biomol NMR* **2024**, *78*, 237−247.
(48) Mochizuki, A.; Saso, A.; Zhao, Q.; Kubo, S.; Nishida, N.; Shimada, I. Balanced Regulation of Redox Status of Intracellular Thioredoxin Revealed by In-Cell NMR. *J. Am. Chem. Soc.* **2018**, *140* (10), 3784−3790.
(49) Leuenberger, P.; Ganscha, S.; Kahraman, A.; Cappelletti, V.; Boersema, P. J.; von Mering, C.; Claassen, M.; Picotti, P. Cell-Wide Analysis of Protein Thermal Unfolding Reveals Determinants of Thermostability. *Science* **2017**, *355* (6327), No. eaai7825.
(50) Ramalingam, N.; Dettmer, U. Temperature Is a Key Determinant of Alpha- and Beta-Synuclein Membrane Interactions in Neurons. *J. Biol. Chem.* **2021**, *296*, No. 100271.
(51) Shchukina, A.; Schwarz, T. C.; Nowakowski, M.; Konrat, R.; Kazimierczuk, K. Non-Uniform Sampling of Similar NMR Spectra and Its Application to Studies of the Interaction between Alpha-Synuclein and Liposomes. *J. Biomol. NMR* **2023**, *77*, 149−163.
(52) Mansueto, S.; Fusco, G.; De Simone, A. α-Synuclein and Biological Membranes: The Danger of Loving Too Much. *Chem. Commun.* **2023**, *59* (57), 8769−8778.
(53) Lokappa, S. B.; Suk, J.-E.; Balasubramanian, A.; Samanta, S.; Situ, A. J.; Ulmer, T. S. Sequence and Membrane Determinants of the Random Coil−Helix Transition of α-Synuclein. *J. Mol. Biol.* **2014**, *426* (10), 2130−2144.
(54) Fusco, G.; Pape, T.; Stephens, A. D.; Mahou, P.; Costa, A. R.; Kaminski, C. F.; Kaminski Schierle, G. S.; Vendruscolo, M.; Veglia, G.; Dobson, C. M.; De Simone, A. Structural Basis of Synaptic Vesicle Assembly Promoted by α-Synuclein. *Nat. Commun.* **2016**, *7* (1), 12563.
(55) Runwal, G.; Edwards, R. H. The Membrane Interactions of Synuclein: Physiology and Pathology. *Annu. Rev. Pathol. Mech. Dis.* **2021**, *16* (1), 465−485.
(56) Ryder, B. D.; Wydorski, P. M.; Hou, Z.; Joachimiak, L. A. Chaperoning Shape-Shifting Tau in Disease. *Trends Biochem. Sci.* **2022**, *47* (4), 301−313.
(57) El Mammeri, N.; Dregni, A. J.; Duan, P.; Wang, H. K.; Hong, M. Microtubule-Binding Core of the Tau Protein. *Sci. Adv.* **2022**, *8* (29), No. eabo4459.
(58) Boyko, S.; Surewicz, W. K. Tau Liquid−Liquid Phase Separation in Neurodegenerative Diseases. *Trends in Cell Biology* **2022**, *32* (7), 611−623.
(59) Bok, E.; Leem, E.; Lee, B.-R.; Lee, J. M.; Yoo, C. J.; Lee, E. M.; Kim, J. Role of the Lipid Membrane and Membrane Proteins in Tau Pathology. *Front. Cell Dev. Biol.* **2021**, *9*, No. 653815.
(60) Sallaberry, C. A.; Voss, B. J.; Majewski, J.; Biernat, J.; Mandelkow, E.; Chi, E. Y.; Vander Zanden, C. M. Tau and Membranes: Interactions That Promote Folding and Condensation. *Front. Cell Dev. Biol.* **2021**, *9*, No. 725241.
(61) Zhuang, S.; Chakraborty, P.; Zweckstetter, M. Regulation of Tau by Peptidyl-Prolyl Isomerases. *Curr. Opin. Struct. Biol.* **2024**, *84*, No. 102739.
(62) Loth, K.; Pelupessy, P.; Bodenhausen, G. Chemical Shift Anisotropy Tensors of Carbonyl, Nitrogen, and Amide Proton Nuclei in Proteins through Cross-Correlated Relaxation in NMR Spectroscopy. *J. Am. Chem. Soc.* **2005**, *127* (16), 6062−6068.
(63) Tang, S.; Case, D. A. Vibrational Averaging of Chemical Shift Anisotropies in Model Peptides. *J. Biomol NMR* **2007**, *38* (3), 255−266.
(64) Jordan, D. M.; Mills, K. M.; Andricioaei, I.; Bhattacharya, A.; Palmo, K.; Zuiderweg, E. R. P. Parameterization of Peptide ^{13}C Carbonyl Chemical Shielding Anisotropy in Molecular Dynamics Simulations. *ChemPhysChem* **2007**, *8* (9), 1375−1385.
(65) Schiavina, M.; Bracaglia, L.; Rodella, M. A.; Kümmerle, R.; Konrat, R.; Felli, I. C.; Pierattelli, R. Optimal 13C NMR Investigation of Intrinsically Disordered Proteins at 1.2 GHz. *Nat. Protoc.* **2024**, *19*, 406.
(66) Shimba, N.; Kovacs, H.; Stern, A. S.; Nomura, A. M.; Shimada, I.; Hoch, J. C.; Craik, C. S.; Dötsch, V. Optimization of 13C Direct Detection NMR Methods. *J. Biomol. NMR* **2004**, *30* (2), 175−179.
(67) Bastawrous, M.; Tabatabaei-Anaraki, M.; Soong, R.; Bermel, W.; Gundy, M.; Boenisch, H.; Heumann, H.; Simpson, A. J. Inverse or Direct Detect Experiments and Probes: Which Are "Best" for in-Vivo NMR Research of 13C Enriched Organisms? *Anal. Chim. Acta* **2020**, *1138*, 168−180.
(68) Theillet, F.-X.; Luchinat, E. In-Cell NMR: Why and How? *Prog. Nucl. Magn. Reson. Spectrosc.* **2022**, *132*−*133*, 1−112.
(69) Ghouil, R.; Bouguechtouli, C.; Chérot, H.; Marcelot, A.; Roche, M.; Theillet, F.-X. Affordable Amino Acid α/β-Deuteration and Specific Labeling for NMR Signal Enhancement: Evaluation on the Kinase P38α. *J. Magn Reson Open* **2023**, *16*−*17*, No. 100126.
(70) Jiménez, J. S. Macromolecular Structures and Proteins Interacting with the Microtubule Associated Tau Protein. *Neuroscience* **2023**, *518*, 70−82.
(71) Tracy, T. E.; Madero-Pérez, J.; Swaney, D. L.; Chang, T. S.; Moritz, M.; Konrad, C.; Ward, M. E.; Stevenson, E.; Hüttenhain, R.; Kauwe, G.; Mercedes, M.; Sweetland-Martin, L.; Chen, X.; Mok, S.-A.; Wong, M. Y.; Telpoukhovskaia, M.; Min, S.-W.; Wang, C.; Sohn, P. D.; Martin, J.; Zhou, Y.; Luo, W.; Trojanowski, J. Q.; Lee, V. M. Y.; Gong, S.; Manfredi, G.; Coppola, G.; Krogan, N. J.; Geschwind, D. H.; Gan, L. Tau Interactome Maps Synaptic and Mitochondrial Processes Associated with Neurodegeneration. *Cell* **2022**, *185* (4), 712−728.e14.
(72) Parra Bravo, C.; Naguib, S. A.; Gan, L. Cellular and Pathological Functions of Tau. *Nat. Rev. Mol. Cell Biol.* **2024**, *25* (11), 845−864.
(73) Jensen, O.; Ansari, S.; Gebauer, L.; Müller, S. F.; Lowjaga, K. A. A. T.; Geyer, J.; Tzvetkov, M. V.; Brockmöller, J. A Double-Flp-in

Method for Stable Overexpression of Two Genes. *Sci. Rep.* **2020**, *10* (1), 14018.
(74) Suppmann, S. Inducible Protein Expression in piggyBac Transposase Mediated Stable HEK293 Cell Pools. *Methods Enzym.* **2021**, *660*, 321−339.
(75) Shin, S.; Kim, S. H.; Lee, J. S.; Lee, G. M. Streamlined Human Cell-Based Recombinase-Mediated Cassette Exchange Platform Enables Multigene Expression for the Production of Therapeutic Proteins. *ACS Synth. Biol.* **2021**, *10* (7), 1715−1727.
(76) Rynes, J.; Istvankova, E.; Dzurov Krafcikova, M.; Luchinat, E.; Barbieri, L.; Banci, L.; Kamarytova, K.; Loja, T.; Fafilek, B.; Rico-Llanos, G.; Krejci, P.; Macurek, L.; Foldynova-Trantirkova, S.; Trantirek, L. Protein Structure and Interactions Elucidated with In-Cell NMR for Different Cell Cycle Phases and in 3D Human Tissue Models. *Commun. Biol.* **2025**, *8* (1), 194.
(77) Lotthammer, J. M.; Ginell, G. M.; Griffith, D.; Emenecker, R. J.; Holehouse, A. S. Direct Prediction of Intrinsically Disordered Protein Conformational Properties from Sequence. *Nat. Methods* **2024**, *21* (3), 465−476.
(78) Skinner, S. P.; Fogh, R. H.; Boucher, W.; Ragan, T. J.; Mureddu, L. G.; Vuister, G. W. CcpNmr AnalysisAssign: A Flexible Platform for Integrated NMR Analysis. *J. Biomol NMR* **2016**, *66* (2), 111−124.

https://doi.org/10.1021/jacs.5c15061
J. Am. Chem. Soc. 2025, 147, 46259−46269